

On the linear theory of Kelvin-Helmholtz instabilities of relativistic magnetohydrodynamic planar flows

Z. Osmanov^{1,*}, A. Mignone^{1,2}, S. Massaglia¹, G. Bodo² and A. Ferrari¹

¹ Dipartimento di Fisica Generale, Università degli Studi di Torino, via Pietro Giuria 1, 10125 Torino
e-mail: name1@to.infn.it

² INAF/Osservatorio Astronomico di Torino, Strada Osservatorio 20, 10025 Pino Torinese, Italy e-mail: name2@oato.inaf.it

Received ; accepted

ABSTRACT

Aims. We investigate the linear stability properties of the plane interface separating two relativistic magnetized flows in relative motion. The two flows are governed by the (special) relativistic equations for a magnetized perfect gas in the infinite conductivity approximation.

Methods. By adopting the vortex-sheet approximation, the relativistic magnetohydrodynamics equations are linearized around the equilibrium state and the corresponding dispersion relation is derived and discussed. The behavior of the configuration and the regimes of instability are investigated following the effects of four physical parameters, namely: the flow velocity, the relativistic and Alfvénic Mach numbers and the inclination of the wave vector on the plane of the interface.

Results. From the numerical solution of the dispersion relation, we find in general two separate regions of instability, associated respectively with the slow and fast magnetosonic modes. Modes parallel to the flow velocity are destabilized only for sufficiently low magnetization. For the latter case, stabilization is attained, additionally, at sufficiently large relativistic velocities between the two flows in relative motion.

Conclusions. The relevance of these results to the study of the stability of astrophysical jets is briefly commented.

Key words. Kelvin-Helmholtz instability - relativistic MHD - plasma physics

1. Introduction

The Kelvin-Helmholtz instability (KHI henceforth), acting at the contact interface between two flows in relative motion, plays a dynamically important role in a number of different astrophysical scenarios such as, for example accretion disks, planetary magnetospheres, stellar and extragalactic jets. It is a classical instability in fluid dynamics, already discussed at the end of nineteenth century in the works of Von Helmholtz & Monats (1868) and Lord Kelvin (1871). The classical results of the linear analysis for incompressible flows separated by a planar vortex sheet, both in the presence of magnetic fields and for different geometries are summarized in Chandrasekhar's monograph (Chandrasekhar 1961). They have been later generalized for compressible case both in the pure hydrodynamical limit (see e.g. Gerwin 1968; Sen 1964) and in the magnetohydrodynamic (MHD) limit (see e.g. Sen 1963; Pu & Kivelson 1983) extending the study to the supersonic regime. In particular it was shown that in the hydrodynamic case no unstable longitudinal (with respect to the plane interface) modes are allowed for flow Mach numbers larger than $\sqrt{8}$, while transverse modes are always unstable.

More recently Choudhury & Lovelace (1986) studied the linear instability behavior in the case of a finite-thickness boundary layer, as a function of the Alfvén velocity and inclination of the wave vector with respect to the interface. Their main result was the proof of the existence of two distinct regimes of instability in the wavevector-Mach number plane correspond-

ing to standing and traveling MHD waves, the extent of the instability regions depending upon the magnetization parameter. Magnetohydrodynamic flows in cylindrical and slab geometries have been studied by Ferrari et al. (1981), (1982) showing the existence of a new range of unstable modes, arising for high Mach number flows, due to standing waves created by reflections at the boundaries of the structures.

For astrophysical problems involving high-energy phenomena relativistic effects become important either because the relative velocities are close to the speed of light or because the plasma is relativistically hot or because the magnetic field is very strong and the Alfvén speed becomes close to the speed of light. For the non magnetic case a relativistic extension of the KHI study was considered, for a plane parallel velocity discontinuity, by Turland & Scheuer (1976), Blandford & Pringle (1976) and more recently by Bodo et al. (2004). In particular Bodo et al. (2004) showed that the dispersion relation can be solved analytically in a frame of reference where the media in the two half-spaces have equal and opposite velocities and that the stability criteria have the same form of classical ones, simply substituting the Mach number with the relativistic Mach number, that was first introduced by Königl (1980).

The relativistic MHD case still lacks of a full stability analysis and this is what we present in this paper. Early attempts were carried out by Ferrari et al. (1980). Their analysis, however, assumed the limit of Alfvén velocity much smaller than the speed of light, thus allowing to neglect displacement currents, while the speed of the flow could reach relativistic values. The main result of this study was the confirmation that KHI disappears when the Alfvén velocity approaches or becomes larger than the

Send offprint requests to: Z. Osmanov

* something

speed of sound and when a large density contrast exists between the two media.

Relativistic magnetized flows can be found in astrophysical environments associated to AGN jets, to jets from galactic X-ray binaries, such as GRS 1915+105 (Mirabel & Rodriguez 1999), and to pulsar wind nebulae (PWNe). Applications of the Kelvin-Helmholtz instability mechanism to the case of AGN and galactic microquasar jets is widely discussed in the literature, mainly for cylindrical geometries, such as the recent analysis by Hardee (2007), who studied axially magnetized cylindrical relativistic jet embedded in a magnetized sheath. In addition KHI appear to be the physical mechanism to slow down relativistic jets by producing entrainment of the ambient medium. Bodo et al. (2003), Rossi et al. (2004) and Rossi et al. (2008) have studied the non-linear evolution of KHI in cylindrical relativistic jets to explain the dichotomy of FRI - FRII extragalactic radiosources. Instead the planar case can apply to the case of PWNe, when a relativistically hot magnetized plasma forms where the pulsar ultra-relativistic wind interacts with the surrounding supernova ejecta. The linear stability analysis that we present here will be relevant for understanding the physical phenomena involved in the destabilization process.

In this work we present, for the first time to our knowledge, a complete treatment of the linear stability problem in the plane-parallel geometry, by considering the full system of equations (i.e. without neglecting the displacement current and accounting for non relativistic as well as relativistic Alfvén velocities). It is shown that the stability properties depend on four physical parameters which we conveniently choose to be the relativistic Mach number, the flow velocity, the Alfvén speed and the inclination of the projection of the wave vector onto the plane of the interface.

The paper is organized as follows. In §2.2 we derive the general dispersion relation, in §3 we present and discuss the results for the non-relativistic and relativistic cases, and we add some astrophysical comments in §4.

2. Relevant Equations

2.1. The Equations of Relativistic MHD

The equations of relativistic magnetohydrodynamics (RMHD henceforth) govern the evolution of a (special) relativistic magnetized fluid. They can be cast as a system of conservation laws, describing energy-momentum and mass conservation:

$$\nabla_\mu T^{\mu\nu} = 0, \quad \nabla_\mu (\rho u^\mu) = 0, \quad (1)$$

where ρ is rest mass density and $u^\mu \equiv (\gamma, \gamma\mathbf{v})$ is the fluid four-velocity ($\gamma \equiv$ Lorentz factor, $\mathbf{v} \equiv$ three velocity) such that $u^\mu u_\mu = -1$. The speed of light is set to unity everywhere. The expression of the energy-momentum tensor can be found under the physical assumptions of constant magnetic permeability and infinite conductivity, appropriate for a perfectly conducting fluid (see, for example, the books by Anile (1989) and Lichnerowicz (1967)).

Under these conditions, the stress energy tensor for a perfect fluid interacting with an electromagnetic field decomposes into $T^{\mu\nu} = T_{\text{FL}}^{\mu\nu} + T_{\text{EM}}^{\mu\nu}$, where the fluid (FL) and electromagnetic (EM) contributions are given, respectively, by

$$T_{\text{FL}}^{\mu\nu} = \rho h u^\mu u^\nu + p \eta^{\mu\nu}, \quad T_{\text{EM}}^{\mu\nu} = F^\mu_\beta F^{\nu\beta} - \frac{1}{4} \eta^{\mu\nu} F_{\alpha\beta} F^{\alpha\beta}. \quad (2)$$

Here h and p are used to denote the gas specific enthalpy and the thermal pressure, while $\eta^{\mu\nu} = \text{diag}(-1, 1, 1, 1)$ is the Minkowski

metric tensor. For ease of notation, factors like 4π have been set to unity in the derivation.

The electromagnetic field tensor $F^{\mu\nu}$ appearing in the definitions of the stress energy tensor, Eq. (2), obeys Maxwell's equations

$$\partial_{[\alpha} F_{\mu\nu]} = 0, \quad \nabla_\mu F^{\mu\nu} = -J^\nu, \quad (3)$$

where [...] denotes anti-symmetrization and J^ν is the charge four-current. In the limit of infinite conductivity, the rest frame electric field vanishes identically and the electromagnetic field tensor becomes orthogonal to the fluid four-velocity, i.e. $F^{\mu\beta} u_\beta = 0$. Note that this is the only approximation introduced in ideal RMHD and it becomes identical to the well known non-relativistic expression $\mathbf{E} = -\mathbf{v} \times \mathbf{B}$, where \mathbf{E} is the electric vector field. Unlike classical MHD, however, the displacement current is not discarded in RMHD and explicitly enters through the definition of the current, given by the second of Eqs. (3). The high conductivity limit allows to write $F^{\mu\nu} = \epsilon^{\alpha\beta\mu\nu} b_\mu u_\nu$, where b^μ is the magnetic induction four-vector:

$$b^\mu = \left[\gamma \mathbf{v} \cdot \mathbf{B}, \frac{\mathbf{B}}{\gamma} + \gamma (\mathbf{v} \cdot \mathbf{B}) \mathbf{v} \right], \quad (4)$$

with \mathbf{B} and $\epsilon^{\alpha\beta\mu\nu}$ denoting the rest frame magnetic field and the Levi-Civita pseudo-tensor, respectively.

For the purpose of our derivation, we explicitly rewrite Eq. (1) in components:

$$\frac{\partial \mathbf{U}}{\partial t} + \sum_{i=1}^3 \frac{\partial \mathbf{f}^i}{\partial x^i} = 0, \quad (5)$$

where \mathbf{U} and \mathbf{f}^i are the vector of conserved variables and corresponding fluxes:

$$\mathbf{U} = [\rho\gamma, w_t \gamma^2 v^j - b^0 b^j, w_t \gamma^2 - b^0 b^0 - p_t]^T, \quad (6)$$

$$\mathbf{f}^i = [\rho\gamma v^i, w_t \gamma^2 v^i v^j - b^i b^j + p_t \delta^{ij}, w_t \gamma^2 v^i - b^0 b^i]^T, \quad (7)$$

where p_t and w_t are, respectively the total pressure and enthalpy, expressed as the sum of thermal and magnetic contributions:

$$p_t = p + \frac{1}{2} |b|^2, \quad w_t = \rho h + |b|^2, \quad (8)$$

where $|b|^2 = b^\alpha b_\alpha$. Magnetic field evolution is given by the induction equation in Maxwell's law:

$$\frac{\partial \mathbf{B}}{\partial t} - \nabla \times (\mathbf{v} \times \mathbf{B}) = 0, \quad (9)$$

which conserves the same form as in the classical case. Proper closure is provided by specifying an equation of state which we take as the constant Γ -law:

$$h = 1 + \frac{\Gamma}{\Gamma - 1} \frac{p}{\rho}, \quad (10)$$

where Γ is the polytropic index of the gas.

2.2. Dispersion Relation

Our setup consists of a planar vortex sheet interface in the xz plane at $y = 0$ separating two uniform flows moving in the x direction with opposite velocities $\mathbf{v}(y > 0) = \beta \mathbf{i}$ and $\mathbf{v}(y < 0) = -\beta \mathbf{i}$. The fluids have equal density and pressure and are threaded by a uniform longitudinal magnetic field along the direction of relative motion, $\mathbf{B} = B_0 \mathbf{i}$.

We start our analysis by introducing small deviations around the equilibrium state. This is better achieved by working in the rest-frames of the fluids, where perturbations are sought in the form:

$$\tilde{\mathbf{B}} = \tilde{\mathbf{B}}_0 + \tilde{\mathbf{B}}' + \dots, \quad (11)$$

$$\tilde{\mathbf{v}} = \tilde{\mathbf{v}}' + \dots, \quad (12)$$

$$\tilde{\rho} = \tilde{\rho}_0 + \tilde{\rho}' + \dots, \quad (13)$$

$$\tilde{p} = \tilde{p}_0 + \tilde{p}' + \dots, \quad (14)$$

where the tilde denotes quantities in the rest frame. The perturbed terms of the first order can be expressed by the following:

$$\tilde{\Psi}'_{\pm} \propto \exp \left[i (\tilde{k}_{\pm} \tilde{x} + \tilde{l}_{\pm} \tilde{y} + \tilde{m}_{\pm} \tilde{z} - \tilde{\omega}_{\pm} \tilde{t}) \right], \quad (15)$$

where $\tilde{\Psi}'_{\pm} = (\tilde{\mathbf{B}}'_{\pm}, \tilde{\mathbf{v}}'_{\pm}, \tilde{\rho}'_{\pm}, \tilde{p}'_{\pm})$. Subscripts + and - correspond to the regions $y > 0$ and $y < 0$, respectively. Wave numbers and frequency are denoted with \tilde{k}_{\pm} , \tilde{l}_{\pm} , \tilde{m}_{\pm} and $\tilde{\omega}_{\pm}$.

Proper linearization of the equations leads to the dispersion relation (Komissarov (1999)):

$$\begin{aligned} & (\tilde{\omega}_{\pm}^2 - \tilde{k}_{\pm}^2 V_A^2) \times \\ & \times \left(\frac{\tilde{\omega}_{\pm}^4}{(\tilde{k}_{\pm}^2 + \tilde{l}_{\pm}^2 + \tilde{m}_{\pm}^2)^2} + \frac{\tilde{\omega}_{\pm}^2 \tilde{\mu}_{\pm}}{\tilde{k}_{\pm}^2 + \tilde{l}_{\pm}^2 + \tilde{m}_{\pm}^2} + \tilde{v}_{\pm} \right) = 0, \end{aligned} \quad (16)$$

$$\tilde{\mu}_{\pm} = C_s^2 + V_A^2 - C_s^2 V_A^2 \frac{\tilde{k}_{\pm}^2 + \tilde{l}_{\pm}^2}{\tilde{k}_{\pm}^2 + \tilde{l}_{\pm}^2 + \tilde{m}_{\pm}^2}, \quad (17)$$

$$\tilde{v}_{\pm} = C_s^2 V_A^2 \frac{\tilde{k}_{\pm}^2}{\tilde{k}_{\pm}^2 + \tilde{l}_{\pm}^2 + \tilde{m}_{\pm}^2}, \quad (18)$$

$$C_s = \sqrt{\frac{\Gamma p_0}{\rho_0 h_0}}, \quad (19)$$

$$V_A = \frac{B_0}{\sqrt{\rho_0 h_0 + B_0^2}}, \quad (20)$$

which allow the propagation of the Alfvén mode

$$\frac{\tilde{\omega}_{A\pm}^2}{\tilde{k}_{A\pm}^2} = V_A^2, \quad (21)$$

and the two magneto-acoustic modes, (i) slow magnetosonic

$$\frac{\tilde{\omega}_{s\pm}^2}{\tilde{k}_{s\pm}^2 + \tilde{l}_{s\pm}^2 + \tilde{m}_{s\pm}^2} = \frac{1}{2} \tilde{\mu}_{s\pm} - \frac{1}{2} [\tilde{\mu}_{s\pm}^2 - 4\tilde{v}_{s\pm}^2]^{1/2}, \quad (22)$$

and (ii) fast magnetosonic

$$\frac{\tilde{\omega}_{f\pm}^2}{\tilde{k}_{f\pm}^2 + \tilde{l}_{f\pm}^2 + \tilde{m}_{f\pm}^2} = \frac{1}{2} \tilde{\mu}_{f\pm} + \frac{1}{2} [\tilde{\mu}_{f\pm}^2 - 4\tilde{v}_{f\pm}^2]^{1/2}. \quad (23)$$

Here C_s and V_A are the sound speed and the Alfvén speed respectively. Notice that both C_s and V_A are invariant under Lorentz boosts in the x -direction.

In order to obtain the dispersion relation in the laboratory frame, one has to transform all the quantities by mean of a Lorentz transformation:

$$\tilde{\omega}_{\pm} = \gamma(\omega \mp k\beta), \quad (24)$$

$$\tilde{k}_{\pm} = \gamma(k \mp \omega\beta), \quad \tilde{l}_{\pm} = l_{\pm}, \quad \tilde{m}_{\pm} = m, \quad (25)$$

so that a generic perturbation in our original frame can be expressed as

$$\Psi'_{\pm} \propto \exp [i (kx + l_{\pm}y + mz - \omega t)]. \quad (26)$$

By substituting Eqs. (24) and (25) into Eq. (21) we derive immediately that the possible roots are always real, hence we may already conclude that the Alfvén mode will not contribute to the instability. In the case of Eqs. (22) and (23) we see instead that the resulting slow and fast magnetosonic modes include both real and imaginary roots, and therefore we expect instability in the parameter domains corresponding to these modes.

Direct substitution into the induction equation (9) and into the y and z components of the momentum equation in (5) yields

$$B_0 \frac{\tilde{k}_{\mp}}{\gamma} B'_{y\pm} + [\omega B_0^2 + \gamma \rho_0 h_0 \tilde{\omega}_{\mp}] v'_{y\pm} - l_{\pm} (p'_{\pm} + B_0 B'_{x\pm}) = 0, \quad (27)$$

$$B_0 \frac{\tilde{k}_{\mp}}{\gamma} B'_{z\pm} + [\omega B_0^2 + \gamma \rho_0 h_0 \tilde{\omega}_{\mp}] v'_{z\pm} - m (p'_{\pm} + B_0 B'_{x\pm}) = 0, \quad (28)$$

$$(\omega \mp k\beta) B'_{x\pm} - B_0 (l_{\pm} v'_{y\pm} + m v'_{z\pm}) = 0, \quad (29)$$

$$(\omega \mp k\beta) B'_{y\pm} + k B_0 v'_{y\pm} = 0, \quad (30)$$

$$(\omega \mp k\beta) B'_{z\pm} + k B_0 v'_{z\pm} = 0, \quad (31)$$

where \tilde{k}_{\mp} and $\tilde{\omega}_{\mp}$ are given by Eqs. (24, 25).

With the aid of Eq. (8) one may express the total pressure perturbation as:

$$p'_{\pm} = p_{\pm} + \frac{l_{\pm} B_0^2 v'_{y\pm}}{\omega \mp k\beta}, \quad (32)$$

and imposing the displacement matching condition at the interface:

$$\frac{v'_{y+}}{\omega - k\beta} = \frac{v'_{y-}}{\omega + k\beta}. \quad (33)$$

and the total pressure continuity ($p'_+ = p'_-$) at the interface, one obtains (together with Eq. 27)

$$\frac{l_+}{l_-} = \frac{\rho_0 h_0 \gamma^2 (\omega - k\beta)^2 + (\omega^2 - k^2) B_0^2}{\rho_0 h_0 \gamma^2 (\omega + k\beta)^2 + (\omega^2 - k^2) B_0^2}. \quad (34)$$

Introducing the dispersion relation of slow and fast magnetosonic waves (see the right bracket of Eq. (16)) and solving for l_{\pm}^2 one gets

$$l_{\pm}^2 = -m^2 + \frac{\tilde{\omega}_{\mp}^2 [(C_s^2 + V_A^2) \tilde{k}_{\mp}^2 - \tilde{\omega}_{\mp}^2] - C_s^2 V_A^2 \tilde{k}_{\mp}^4}{C_s^2 V_A^2 (\tilde{k}_{\mp}^2 + \tilde{\omega}_{\mp}^2) - (C_s^2 + V_A^2) \tilde{\omega}_{\mp}^2}, \quad (35)$$

which, combined with Eq. (34), gives the desired dispersion relation of modes connecting through the planar interface.

A number of considerations can be immediately drawn.

- The dispersion relation obtained by substitution of Eq. (34) into Eq. (35) is an 8-th degree polynomial in ω . However, only 4 out of a total of 8 complex roots do actually satisfy Eq. (34) and thus are physically significant.

- Roots with positive imaginary part of ω identify unstable modes. The growth rate will be more conveniently expressed by the imaginary part of the dimensionless quantity

$$\phi \equiv \frac{\omega}{C_s \sqrt{k^2 + m^2}}; \quad (36)$$

- In the non-relativistic limit (i.e. $\beta \rightarrow 0$, $\rho h \gg p$, B_0^2 and $h \rightarrow 1$) our dispersion relation reduces to the form given by Choudhury & Lovelace (1986) in their equations (7) and (A2a);
- In the limit of vanishing magnetic field Eqs. (34) and (35) simplify considerably and the dispersion relation reduces to the one derived by Bodo et al. (2004) (see their Eqs. (33) and (35));
- For the general case the system of equations Eqs. (34, 35) has to be solved numerically and these results are discussed in the following sections.

3. Results

Our study will examine the instability dependence on 4 parameters: 1) the fluid velocity β (alternatively, the Lorentz factor γ), 2) the relativistic Mach number

$$\mathcal{M}_r = \frac{\beta}{C_s} \frac{\sqrt{1 - C_s^2}}{\sqrt{1 - \beta^2}}, \quad (37)$$

3) the Alfvénic Mach number $\zeta = V_A/C_s$ and 4) the ratio $f = m/k$, that gives the angle between the wave number projection on the xz plane and the flow velocity. In general, relativistic effects come into play whenever one of β , \mathcal{M}_r or ζ (or a combination of them) describes situations of high fluid velocities, hot gas or strong magnetic field, respectively. To this purpose, it is useful to use the explicit relation linking the Alfvén speed and the other parameters:

$$V_A = \frac{\beta \zeta}{\sqrt{\beta^2 + \mathcal{M}_r^2 (1 - \beta^2)}}. \quad (38)$$

In the following, we will discuss the non-relativistic case and subsequently the relativistic case, both for oblique propagation ($f \neq 0$) and for propagation parallel to the velocity interface ($f = 0$). The latter case will be useful for the comparison with the results obtained by previous investigators.

3.1. Non-relativistic flows

As a starting point, let us now consider the case of a non-relativistic fluid, with $\beta = 10^{-3}$ and $\Gamma = 5/3$.

A convenient way to gain a comprehensive view of the general behavior of the instability, when one allows for non-parallel propagation (i.e. $f \neq 0$, see also Gerwin (Gerwin 1968), Choudhury & Lovelace (1986)), is to represent the results on a contour plot such as the one in Fig. 1, where the contour levels show the growth rate $\text{Im}(\phi)$ as a function of f and \mathcal{M}_r , for fixed Alfvén Mach number $\zeta = 1.6$ (top panel). From the plot, one derives that i) two separate instability regions are present in the plane (\mathcal{M}_r, f) , corresponding to slow and fast magnetosonic unstable modes, and ii) they do not extend to the horizontal axis, i.e. at $f = 0$. By expanding the solution of the dispersion relation in terms of $1/f$, one can show from Eqs. (34, 35) that the cor-

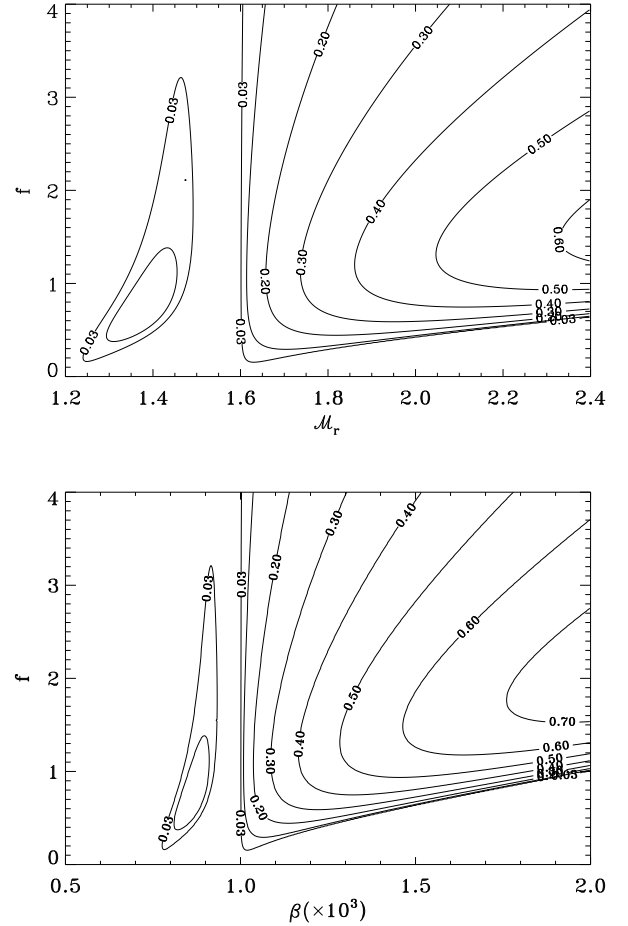


Fig. 1. Two contour plots are shown. Top panel: the contour plot of constant $\text{Im}(\phi)$ surfaces as a function of the inclination factor f and relativistic Mach number \mathcal{M}_r for fixed Alfvénic Mach number $\zeta = 1.6$ and flow velocity $\beta = 10^{-3}$. Bottom panel: the contour plot of constant $\text{Im}(\phi)$ surfaces as a function of the inclination factor f and β for the fixed Alfvén speed ($V_A = 10^{-3}$) and the sound speed ($C_s = 6.3 \times 10^{-4}$). Here $\Gamma = 5/3$ is used.

responding first order term of the growth rate can be expressed by:

$$\phi \sim \frac{1}{f} \left[\frac{V_A^2 - \beta^2}{1 - \beta^2 V_A^2} \right]^{\frac{1}{2}}. \quad (39)$$

Eq. (39) demonstrates that, for large values of f , the instability appears when $V_A < \beta$. In Fig. 1 (bottom panel) we show the contour plot of constant $\text{Im}(\phi)$ surfaces as a function of f and β for $V_A = 10^{-3}$ and $C_s = 6.3 \times 10^{-4}$ (this value corresponds to $\mathcal{M}_r = 1.6$ (top panel), see Eq. 37), and the figure shows that the instability appears for $\beta > 10^{-3}$, i.e. when β exceeds the value of Alfvén speed parameter. We note as well that, while the result in Eq. (39) has a general validity, in the non relativistic limit $\beta \ll 1$, the condition for instability derived above for large f 's reads also $\zeta < \mathcal{M}_r$, as evident for Fig. 1 (top panel).

For smaller f 's, i.e. for small inclinations of the propagation direction with respect to the velocity interface, Fig. 1 shows that for $f \lesssim 0.2$ the system becomes stable for the set of parameters considered.

This general behavior is better understood by looking at the real and imaginary parts of the roots giving rise to unstable

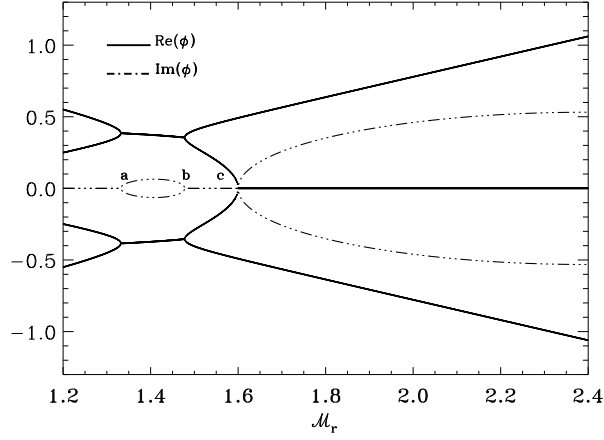


Fig. 2. Imaginary (dotted-dashed lines) and real (solid lines) parts of the roots satisfying the dispersion relation as functions of the relativistic Mach number. Only roots associated with unstable modes are plotted. For the sake of clarity, unphysical roots have been plotted as well. The other parameter set: $\beta = 10^{-3}$, $\zeta = 1.6$, $f = 1$ and $\Gamma = 5/3$. Instability arises when $a < \mathcal{M}_r < b$ and $\mathcal{M}_r > c$.

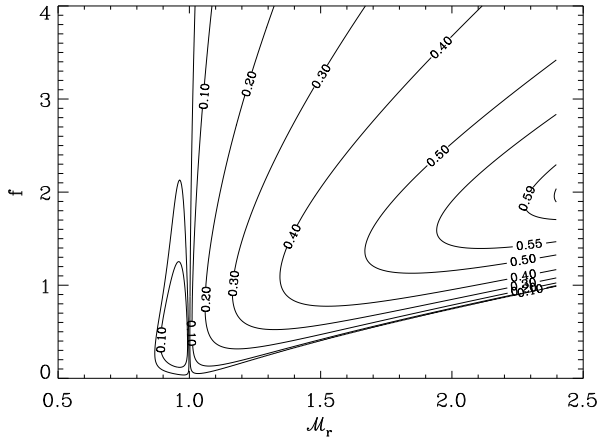


Fig. 3. Same as Fig. 1, but for $\zeta = 1$.

modes, shown in Fig. 2. This plot corresponds to a horizontal cut across the contour lines of Fig. 1 for fixed $f = 1$. Indeed, for $\mathcal{M}_r < a$, all roots are real yielding a stable configuration. For $a < \mathcal{M}_r < b$, however, the roots become complex conjugate with nonzero imaginary parts, making this range unstable. Between $b < \mathcal{M}_r < c$ we have again a stable configuration, whereas for $\mathcal{M}_r > c$ the roots become purely imaginary and a second unstable region can be recognized. It can be verified by direct substitution into Eq. (22) and Eq. (23) that the two family of solutions separately correspond to the onset of slow (for $a < \mathcal{M}_r < b$) and fast ($\mathcal{M}_r > c$) magnetosonic modes, respectively.

For decreasing magnetization (i.e. lower values of ζ), the two instability regions approach each other, gradually shifting towards lower values of \mathcal{M}_r . At the same time, lower values of f become prone to instability, see Fig. 3. The limiting case $f = 0$ is reached for $\zeta < 1$, when the previously identified instability ranges merge into a single unstable region.

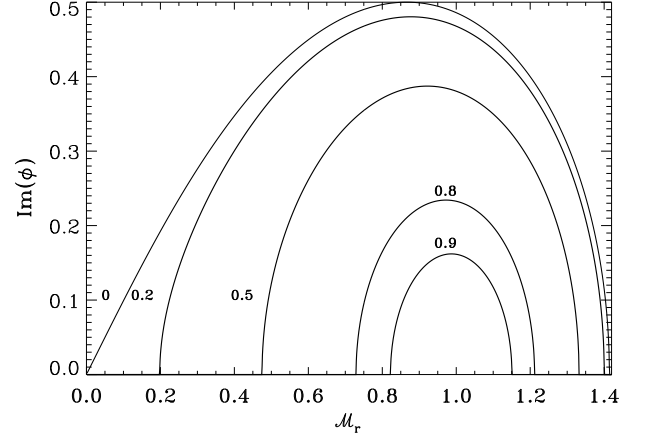


Fig. 4. Dependence of $\text{Im}(\phi)$ on the relativistic Mach number for fixed $\beta = 10^{-3}$ and $f = 0$ ($\Gamma = 5/3$). The different labels above each curve give the values of the Alfvénic Mach number $\zeta = [0, 0.2, 0.5, 0.8, 0.9]$.

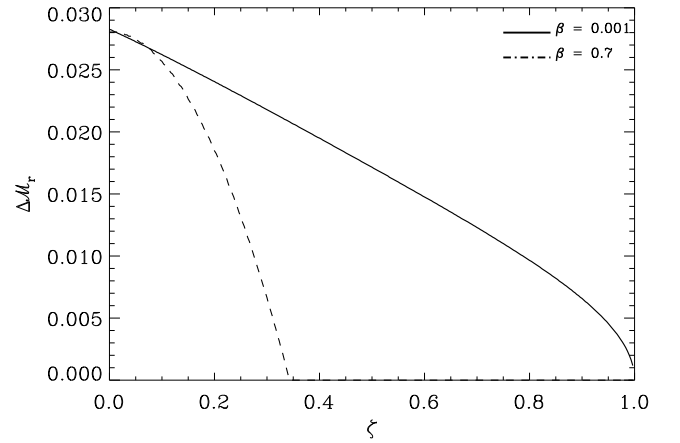


Fig. 5. Instability Mach range $\Delta\mathcal{M}_r$ as a function of the magnetic field in the case of parallel propagation for $\beta = 10^{-3}$ (solid line, $\Gamma = 5/3$) and $\beta = 0.7$ (dashed line, $\Gamma = 4/3$). For the sake of comparison, the latter has been reduced by a factor of 50. Clearly, the instability is suppressed when the Alfvénic Mach number equals to 1 (for $\beta = 10^{-3}$) and 0.35 (for $\beta = 0.7$).

We will now examine the case of parallel propagation ($f = 0$) for different values of $\zeta < 1$. These results may be directly compared with those obtained by Ferrari et al. (1980). In Fig. 4 we plot the growth rate as a function of \mathcal{M}_r for several values of the Alfvénic Mach number in the range $0 \leq \zeta \leq 0.9$. For vanishing magnetic field ($\zeta = 0$) the instability disappears when $\mathcal{M}_r > \sqrt{2}$, consistently with the results shown by Bodo et al. ((2004)). As the magnetic field increases, higher values of ζ induce a stabilizing effect by raising the pressure and forcing the flow to be channeled along the field lines. This has two noticeable effects: one is to decrease the maximum value attained by the growth rate and the other is narrowing down the instability Mach range $\Delta\mathcal{M}_r \equiv \mathcal{M}_r^{\max} - \mathcal{M}_r^{\min}$, where \mathcal{M}_r^{\max} (\mathcal{M}_r^{\min}) is the largest (smallest) value of the Mach number above (below) which the configuration is stable. Note that the values of the sound speed at the growth rate maxima are not relativistic.

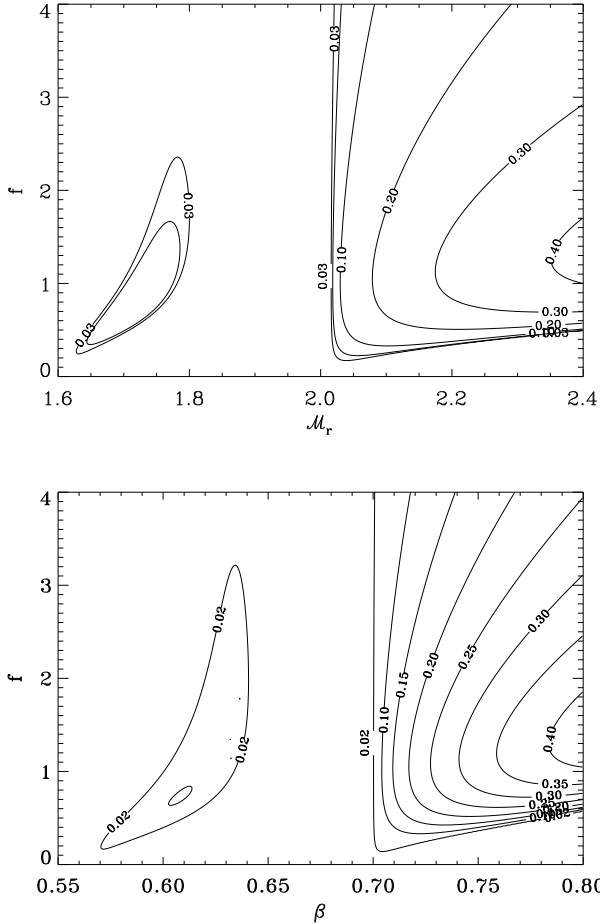


Fig. 6. Top panel: contour plots of constant $\text{Im}(\phi)$ lines in the $M_r - f$ plane for $\beta = 0.7$, $\zeta = 1.6$. The two instabilities branches are clearly visible. Bottom panel: contour plots of constant $\text{Im}(\phi)$ lines in the $\beta - f$ plane for $V_A = 0.7$, $C_s = 0.43$. Here $\Gamma = 4/3$ was used.

Fig. 5 shows the dependence of the critical range of the relativistic Mach number on the magnetic field (solid line). As it is clear from the plot, when $\zeta \rightarrow 1$, the relativistic Mach number range tends to zero and the instability disappears. For $\zeta > 1$ the interface is always stable. Our results are thus in full agreement with those of Ferrari et al. (1980) for the same parameter range ($\beta = 10^{-3}$, $f = 0$).

3.2. Relativistic flows

In the previous subsection all the relevant quantities were describing essentially flows in non-relativistic conditions. We now consider situations in which the fluid exhibits relativistic behavior, at least in some parameter range.

The top panel in Fig. 6 shows the contour levels of the growth rate for fixed flow velocity $\beta = 0.7$ and Alfvénic Mach number $\zeta = 1.6$. We have again a slow magnetosonic modes instability region for $1.63 < M_r < 1.8$, and a fast magnetosonic modes instability one for $M_r > 2.02$. For large f 's the latter one only survives and the discussion for the non relativistic case is still valid, i.e. the instability condition is $V_A < \beta$ (see Fig. 6 bottom panel). In fact, a direct comparison between Figs. 6 and 1 reveals a similar qualitative behavior between the two instabil-

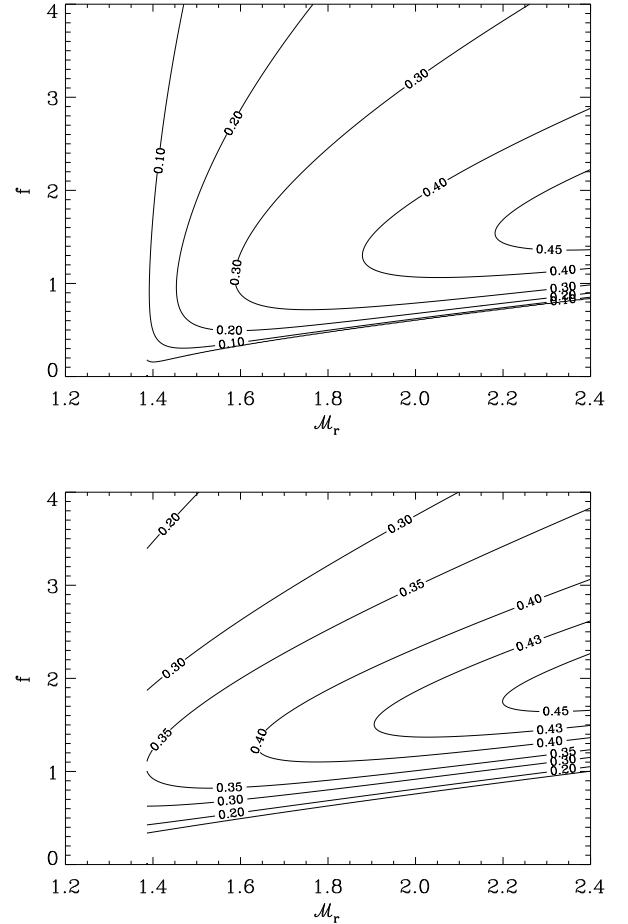


Fig. 7. Contour plots of constant $\text{Im}(\phi)$ lines in the $M_r - f$ plane for $\beta = 0.7$, $\zeta = 1.2$ (top panel) and $\zeta = 1$ (bottom panel). Here $\Gamma = 4/3$ was used.

ity regions corresponding to slow and fast magnetosonic modes. Indeed, in the relativistic case, higher values of M_r are necessary to promote instability and the gap separating the two regions becomes larger. However, for lower values of ζ , only one instability region survives and there are no contour lines for $M_r < 1.4$, see the top panel in Fig. 7. This is a consequence of the fact that higher values of the relativistic Mach number correspond to lower sound speeds and, since the latter cannot exceed the upper limiting value of $1/\sqrt{3}$, M_r has a lower physical cutoff at $\sqrt{2}\beta\gamma \approx 1.386$. Thus, no merging can take place as ζ decreases, since the leftmost region disappears below this threshold. This effect is clearly visible in Fig. 7. In the limit of parallel propagation ($f = 0$), the growth rate decreases with stronger magnetization, see Fig. 8. This is also manifested by a reduced range of the Mach number values for which instability exists. This behavior has already been discussed for non-relativistic flows in §3.1, where the flow was shown to become stable for values of the Alfvén speed close to the speed of sound. For the present case ($\beta = 0.7$), however, stability is approached when the Alfvén speed $V_A \approx 0.35C_s$, see Fig. 8. This tendency can also be recognized by the profile of ΔM_r (the critical Mach number instability range) as function of ζ shown in Fig. 5 (dashed line). As anticipated, the instability is quenched for $\zeta \approx 0.35$, an effect which can also be justified by the increased kinematic inertia.

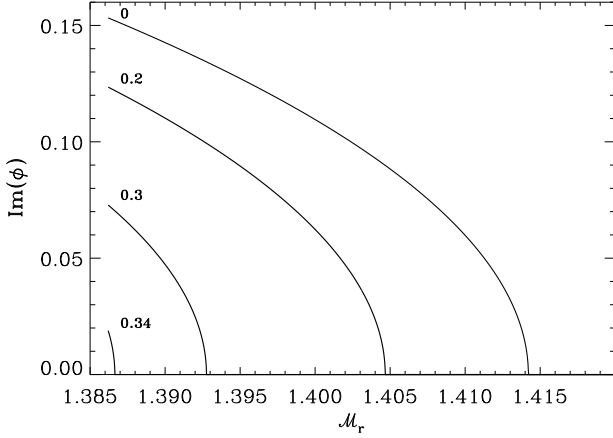


Fig. 8. Effects of magnetic field on the growth rate. Labels on each curve indicate values of ζ . The set of parameters is: $\beta = 0.7$, $\zeta = [0, 0.2, 0.3, 0.34]$, $f = 0$ and $\Gamma = 4/3$. For $\zeta = 0.35$ the flow is completely stabilized.

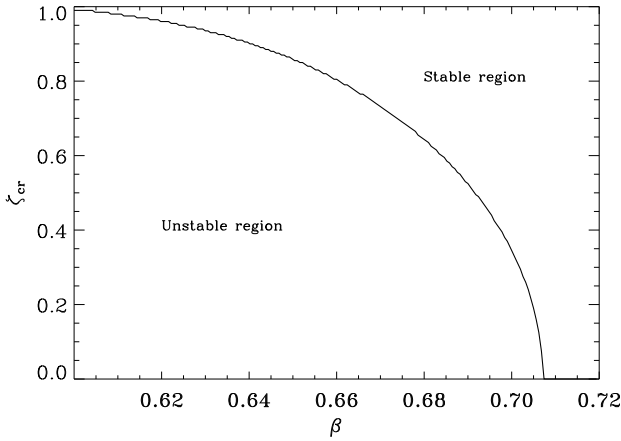


Fig. 9. Effect of the kinematic factor on the instability when $f = 0$ ($\Gamma = 4/3$). As it is clear, for $\beta \approx 0.71$ the instability is suppressed by relativistic effects independently on M_r .

These results confirm the general trend already discussed in (1980); however differences in the growth rates are found when the Alfvén velocity approaches the velocity of light and displacements currents become relevant.

In Fig. 9, indeed, we show the critical value of ζ (above which the instability is suppressed) as a function of the flow velocity β . Thus ζ_{cr} monotonically decreases from ~ 1 (at $\beta = 0.6$) to 0 for $\beta \approx 0.71$. Higher value of β leads to a stable interface, even without magnetic fields. This is a major difference from the classical MHD case. The latter result was already introduced by Bodo et al. ((2004)), where it was shown that positive growth rates are subject to the condition

$$\beta < C_s \left[\frac{2}{1 + C_s^2} \right]^{\frac{1}{2}}. \quad (40)$$

Since the right hand side is a monotonically increasing function of C_s , we conclude that for $\beta \geq 0.7071$ ($C_s = 1/\sqrt{3}$) the instability is suppressed by kinematic effects only, regardless of the value of the magnetic field.

4. Summary

We carried out a linear stability analysis of the relativistic magnetized Kelvin-Helmholtz instability problem in the vortex sheet approximation. Solutions to the dispersion relation have been sought in terms of four parameters giving the strength of the magnetic field, the relativistic Mach number, the flow velocity and the spatial orientation of the wave vector. The main results of this analysis can be summarized as follows:

1. We have examined the cases of non-relativistic and relativistic flows separately. We have found that, for fixed values of the Alfvén velocity, two separate regions of instability appear in the plane (M_r, f) . These two instability regions are associated with the destabilization of slow and fast magnetosonic modes. For large f 's, only the fast magnetosonic modes are unstable in the region $V_A < \beta$.
2. For high values of the Alfvén velocity, modes propagating parallel to the flow velocity are stable. As this velocity decreases, the two instability regions corresponding to slow and fast magnetosonic modes tend to merge and the parallel modes eventually destabilize. This general behavior is common for both non-relativistic and relativistic flows.
3. We have found that slow modes non-parallel to the flow direction are gradually excluded from the instability plane as they become unphysical. This effect takes place for increasing relativistic velocities or low magnetic fields or a combination of both.
4. When considering the case of parallel propagation ($f = 0$), we have found that, similar to the non-magnetic counterpart, the flow becomes linearly stable when the relativistic Mach number exceeds a critical value. In the limit of vanishing Lorentz force, this threshold reaches the maximum value of $\sqrt{2}$, in a frame where the fluids have equal and opposite velocities.
5. For increasing magnetic field strength, the maximum unstable growth rate decreases and the instability exists for a narrow range of Mach number values.
6. The main difference from the non relativistic MHD is that, at higher flow velocities (for $f = 0$), kinematic effects stabilize the flow even for smaller values of the Alfvén velocity. Furthermore, the computed growth rates attain lower values than their classical counterparts. When the flow velocity becomes higher than $1/\sqrt{2}$, the flow does not need any more the magnetic field for stabilization.

Relativistic flows stabilize the KH modes due to the concurrence of two effects: first, at high relative velocities, the mode coupling between the two half-spaces loosens because of causality effects, this effect is present in the non-relativistic case as well but is even more relevant at relativistic velocities; second, in the relativistic regime the inertia of the fluid particles is dynamically augmented, hampering the response of the fluid to the instability.

Destabilization of relativistic Kelvin-Helmholtz modes has been applied in the astrophysical context of jets of extended extragalactic radiosources and relativistic galactic sources to explain the generation of observed morphologies and the driving mechanisms for their radiation emission. While originally these modes were thought to yield disruption of the collimated propagation, it was later realized that the head of jets creates a bow shock and a cocoon that shield the flow from steep gradient boundary layers while leading to generation of a turbulent state. Turbulence is functional in producing mixing of jet and ambient matter with entrainment, angular momentum transport and slowing down of the flow (Rossi et al. 2008). The behavior of

KHI as a function of the physical parameters is likely to be at the base of the different classes of radiosources. In addition long wavelength modes may develop and generate global structures as the wiggles and knots that are observed in astrophysical jets. The present fully relativistic analysis confirms that in order to activate KH modes small V_A/C_S ratios are needed. This condition can be realized in particular by very hot plasmas, even for relatively large magnetic fields, as it appears to be the case in high-energy sources.

KHI appears also to be relevant in the case of PWNe; in fact in these objects a relativistically hot magnetized plasma is produced by the pulsar ultra-relativistic wind and interacts with the surrounding supernova ejecta. These PWNe are internally structured and presents high velocity flow channels that can become KH unstable. As already mentioned, Bucciantini & Del Zanna (2006) have examined numerically the nonlinear development of KHI in these channels, assuming planar geometry, for interpreting the signature of the instability on the synchrotron emission. The present linear stability analysis is complementary to their study as it allows a better comprehension of the physical phenomena involved in the destabilization process. Again the presence of a hot plasma appears necessary to start the channel destabilization.

Acknowledgements. The authors are grateful to Dr. Edoardo Trussoni for valuable discussions. The research was partially supported by the Georgian National Science Foundation grant GNSF/ST06/4-096.

References

- Anile A. M., 1989, *Relativistic fluids and Magneto-Fluids*, Cambridge Univ. Press, Cambridge
- Blandford R. & Pringle J., 1976, *Mon. Not. R. Astron. Soc.*, **176**, 443
- Bodo, G., Rossi, P., Mignone, A., Massaglia, S., & Ferrari, A. 2003, *New Astronomy Review*, **47**, 557
- Bodo G., Mignone A. & R. Rosner, 2004, *Phys.Rev.E* **70**,036304
- Bucciantini N. & Del Zanna L., 2006, *A&A*, **454**, 393
- Chandrasekhar, S., 1961, *Hydrodynamic and Hydromagnetic Stability*, Oxford: Clarendon
- Hardee, P. E. 1987, *ApJ* , 313, 607
- Hardee, P. E. 2007, *ApJ* , 664, 26
- Ferrari A., Trussoni E., & Zaninetti L., 1980, *Mon. Not. R. Astron. Soc.*, **193**, 469
- Ferrari A., Trussoni E., & Zaninetti L., 1981, *Mon. Not. R. Astron. Soc.*, **196**, 1051
- Ferrari A., Massaglia, S. & Trussoni E., 1982, *Mon. Not. R. Astron. Soc.*, **198**, 1065
- Gerwin R.A., 1968, *Rev. Mod. Phys.* **40**, 652
- Komissarov S.S., 1999, *Mon. Not. R. Astron. Soc.*, **303**, 343
- Königl, A., 1980, *Phys. Fluids*, **23**, 1083.
- Lord Kelvin, 1871, *Philos. Mag.* **42**, 362
- Lichnerowicz, A. 1967, *Relativistic Hydrodynamics and Magnetohydrodynamics*, New York: Benjamin,
- Mirabel, I.F., Rodriguez, L.F., 1999, *ARA&A*, **37**, 409
- Pu, Z.Y., & Kivelson, M.G., 1983, *J.Geophys.Res.*, **88**, 841
- Roy S. Choudhury, & Lovelace R.V., 1986, *ApJ*, **302**, 188
- Rossi, P., Bodo, G., Massaglia, S., Ferrari, A., & Mignone, A. 2004, *ApSS*, **293**, 149
- Rossi, P., Mignone, A., Bodo, G., Massaglia, S., & Ferrari, A. 2008, *A&A*, in press
- Sen, A.K., 1963, *Phys. Fluids*, **6**, 1154
- Sen, A.K., 1963, *Phys. Fluids*, **7**, 1293
- Turland B.D. & Scheuer P.A.G., 1976, *Mon. Not. R. Astron. Soc.*, **176**, 421
- Von Helmholtz H., *Monats K.*, 1868, *Preuss. Akad. Wiss. Berlin* **23**, 215